Inorganic Chemistry

pubs.acs.org/IC

Article

d^6*versus* d^{10}, Which Is Better for Second Harmonic Generation Susceptibility? A Case Study of $K_2TGe_3Ch_8$ (T = Fe, Cd; Ch = S, Se)

Bingheng Ji, Fei Wang, Kui Wu, Bingbing Zhang,* and Jian Wang*

Cite This: *Inorg. Chem.* 2023, 62, 574−582

Read Online

ACCESS | Metrics & More | Article Recommendations | Supporting Information

ABSTRACT: Two acentric chalcogenide compounds, $K_2CdGe_3S_8$ and $K_2CdGe_3Se_8$, were synthesized *via* conventional high-temperature solid-state reactions. The crystal structures of $K_2CdGe_3S_8$ and $K_2CdGe_3Se_8$ were accurately determined by single-crystal X-ray diffraction and crystallize in the $K_2FeGe_3S_8$ structure type. $K_2CdGe_3S_8$ is isostructural to $K_2FeGe_3S_8$ with superior nonlinear optical properties. For the second harmonic generation (SHG) response, $K_2CdGe_3S_8$ is 18× $K_2FeGe_3S_8$ for samples of particle size of 38−55 μm. The superior nonlinear optical properties of $K_2CdGe_3S_8$ over $K_2FeGe_3S_8$ are mainly contributed by the chemical characteristics of Cd compared with Fe, which are elucidated by nonlinear optical property measurements, electronic structure calculations, and density functional theory calculations. The [CdS_4] tetrahedra within $K_2CdGe_3S_8$ exhibit a higher degree of distortion and larger volume compared to the [FeS_4] tetrahedra in $K_2FeGe_3S_8$. This study possesses a good platform to investigate how d-block elements contribute to the SHG response. The fully occupied d^{10}-elements are better for SHG susceptibility than d^6-elements in this study. $K_2CdGe_3S_8$ is a good candidate as an infrared nonlinear optical material of high SHG response (2.1× $AgGaS_2$, samples of particle size of 200−250 μm), type-I phase-matching capability, high laser damage threshold (6.2× $AgGaS_2$), and good stability.

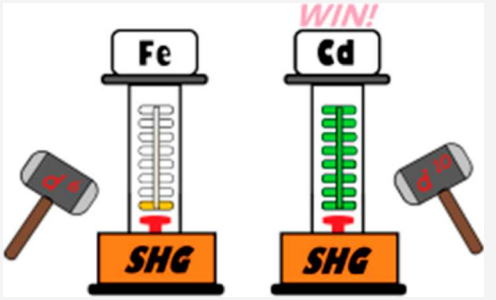

INTRODUCTION

Infrared nonlinear optical materials, which are utilized to generate infrared lasers *via* the second harmonic generation (SHG) process, keep sparking new research interest.[1−13] A promising infrared nonlinear optical material should balance a list of criteria, including large SHG coefficients, high laser damage threshold (LDTs), capability of phase matching, high thermal- and air-stability, and easy growth into a large crystal.[1−13] Within these parameters, SHG coefficients are extremely important due to the correlation between energy conversion efficiency and SHG coefficients, where the bigger SHG coefficients result in a higher overall energy conversion efficiency.[1−13]

To enhance SHG coefficients, some strategies such as incorporating elements with a stereoactive lone electron pair[14−18] and a conjugated structure motif[19−24] have proved effective. In the contrast, the elements that needed to be avoided would be elements with d−d transitions present.[25−38] In this work, we reported an acentric chalcogenide system of $K_2TGe_3Ch_8$ (T = Fe, Cd; Ch = S, Se), which provides a good platform for studying how d electron configuration affects SHG coefficients. $K_2CdGe_3S_8$ and $K_2CdGe_3Se_8$ are new members of the $II_2II_1IV_3Ch_8$ (II = K, Rb, Cs; II = Mn, Co, Fe, Zn, Cd; IV = Ge, Sn; and Ch = S, Se) family.[25−38] $K_2CdGe_3S_8$ and $K_2CdGe_3Se_8$ are isostructural to $K_2FeGe_3S_8$. $K_2CdGe_3S_8$ and $K_2CdGe_3Se_8$ possess superior nonlinear optical (NLO) properties compared to $K_2FeGe_3S_8$. For SHG coefficients, $K_2CdGe_3S_8$ and $K_2CdGe_3Se_8$ are 18× and 4.4× $K_2FeGe_3S_8$, respectively (samples of particle size of 38.5−54 μm). $K_2CdGe_3S_8$ and $K_2CdGe_3Se_8$ are type-I phase-matching materials. $K_2CdGe_3S_8$ exhibits balanced NLO properties of a high SHG coefficient (2.1× $AgGaS_2$, samples of particle size of 200−250 μm), high LDTs (6.2× $AgGaS_2$), and good air stability and is the record holder of best SHG properties in the $II_2II_1IV_3Ch_8$ (II = K, Rb, Cs; II = Mn, Co, Fe, Zn, Cd; IV = Ge, Sn; and Ch = S, Se) family.[25−38] The superior SHG response of $K_2CdGe_3S_8$ is attributed to the chemical characteristics of Cd compared to Fe, which was studied in this work. A detailed study of crystal structures, electronic structures, optical properties, and density functional theory (DFT) calculations of $K_2TGe_3Ch_8$ (T = Fe, Cd and Ch = S, Se) is summarized in the present work.

EXPERIMENTAL PROCEDURES

Synthesis. All starting materials were stored in an argon-filed glovebox with the oxygen level below 0.5 ppm. All starting materials were of commercial grade and used without any further purifications: potassium (Alfa Aesar, 99.95%), cadmium shot (Alfa Aesar, 99.95%),

Received: November 1, 2022
Published: December 27, 2022

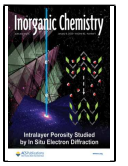

https://doi.org/10.1021/acs.inorgchem.2c03852
Inorg. Chem. 2023, 62, 574−582

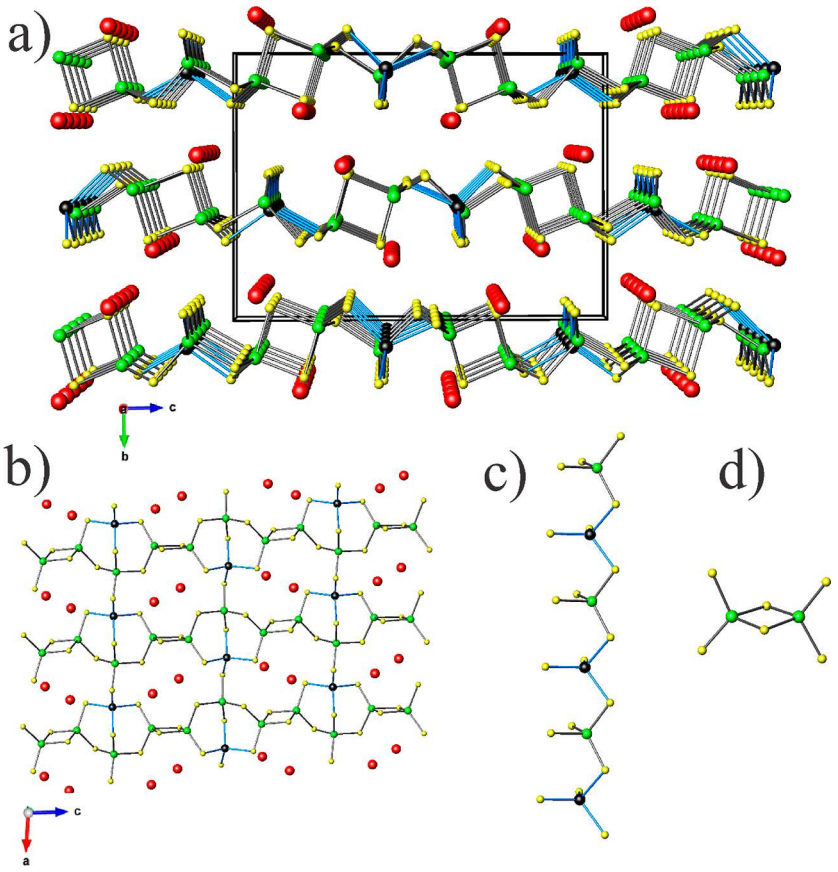

Figure 1. (a) Ball-stick crystal structures of $K_2CdGe_3S_8$ viewed along the [100] direction, (b) detailed view of $[K_2CdGe_3S_8]$ slabs viewed along the [010] direction, (c) detailed view of the $[CdGeS_6]$ chain, and (d) detailed view of $[Ge_2S_6]$ motifs. K: red color, Cd: black color, Ge: green color, and S: yellow color.

germanium pieces (Alfa Aesar, 99.999%), sulfur powder (Alfa Aesar, 99.5%), and selenium shot (Alfa Aesar, 99.999%).

The crystals of $K_2CdGe_3Q_8$ (Q = S and Se) were synthesized using a solid state method in a stoichiometric ratio (K/Cd/Ge/Q = 2/1/3/8, Q = S, and Se). A total of 0.4 g of elements were loaded under vacuum in flame-sealed silica ampules and placed in a programmable furnace. The bottom of silica ampules was coated with amorphous carbon (thermal decomposition of acetone) to prevent a chemical reaction between K and SiO_2. The ampules were heated from room temperature to 1073 K in 20 h and kept at this temperature for 96 h. Then, the furnace was turned off and naturally cooled to room temperature. The crystals of $K_2CdGe_3S_8$ were transparent light yellow, and that of $K_2CdGe_3Se_8$ was yellow-orange (Figure S1). The quality of crystals of $K_2CdGe_3Se_8$ was improved *via* a second annealing with a slow cooling process. Both $K_2CdGe_3S_8$ and $K_2CdGe_3Se_8$ are stable in dry air for many weeks with no detection of change from powder X-ray diffraction results.

Single-Crystal X-ray Diffraction. Suitable crystals were manually picked up under an optical microscope and mounted to the Rigaku XtaLAB Synergy-I instrument. The data collection was performed at room temperature. The data collection and integration were carried out by CrysAlis^{Pro} software.[39] Details of the data collection and structure refinement are provided in Table S1. Atomic coordinates and selected bond distances are listed in Tables S2 and S3. Crystallographic data for $K_2CdGe_3Ch_8$ (Ch = S, Se) have been deposited to the Cambridge Crystallographic Data Centre, CCDC, 12 Union Road, Cambridge CB21EZ, UK. Copies of the data can be obtained free of charge by quoting the depository numbers CCDC—2177915 ($K_2CdGe_3S_8$) and CCDC—2177916 ($K_2CdGe_3Se_8$). Please notice that the crystals of $K_2CdGe_3Ch_8$ (Ch = S, Se) exhibited an extremely highly twinned nature, which made the crystal structure determination challenging. Many crystals were selected and measured. Few structure models were established during the structure refinement process due to their highly twinned nature. The correct structure models were selected with the aid of high-resolution room temperature synchrotron X-ray diffraction data (*vide infra*).

Laboratory Powder X-ray Diffraction and 11-BM Data. Powder X-ray diffraction data were collected at room temperature using a Rigaku MiniFlex II diffractometer with Cu Kα radiation (λ = 1.5406 Å) in the range 2θ = 10−80°, at a scan step of 0.04° with 10 s exposure time. High-resolution room-temperature synchrotron X-ray diffraction data were collected at beamline 11-BM (calibrated wavelength λ = 0.458935 Å) at the Advanced Photon Source (APS) at the Argonne National Laboratory (ANL). The samples of $K_2CdGe_3Ch_8$ (Ch = S, Se) were verified as single-phase samples by both laboratory powder X-ray diffraction measurements and synchrotron X-ray powder diffraction results (Figures S2−S5).

UV−Vis Measurements. Diffuse-reflectance spectra were recorded at room temperature by a PERSEE-T8DCS UV−vis spectrophotometer equipped with an integration sphere in the wavelength range of 230−850 nm. The reflectance data, R, were recorded and converted to the Kubelka−Munk function, $f(R) = (1 - R)^2(2R)^{-1}$. Tauc plots, $(KM \times E)^2$ and $(KM \times E)^{1/2}$, were applied to estimate direct and indirect band gaps, respectively.

Second Harmonic Measurements. Using the Kurtz and Perry method,[40] powder SHG responses of $K_2CdGe_3Ch_8$ (Ch = S, Se) compounds were investigated by a Q-switch laser (2.09 μm, 3 Hz, 50 ns) with various particle sizes, including 38.5−54, 54−88, 88−105, 105−150, and 150−200 μm. Homemade $AgGaS_2$ was selected as the reference. The laboratory-synthesized $AgGaS_2$ crystals were ground to the same size range as $K_2CdGe_3Ch_8$ (Ch = S, Se). The LDTs of the title compounds were evaluated on powder samples (150−200 μm) with a pulsed YAG laser (1.06 μm, 10 ns, 10 Hz). The judgment criterion is as follows: with increasing laser energy, the color change of

https://doi.org/10.1021/acs.inorgchem.2c03852
Inorg. Chem. 2023, 62, 574−582

the powder sample is constantly observed by an optical microscope to determine the damage threshold. To adjust different laser beams, an optical concave lens is added to the laser path. The damaged spot is measured by the scale of the optical microscope.

DFT Calculations. The electronic structures and optical properties of $K_2FeGe_3S_8$ and $K_2CdGe_3S_8$ were calculated based on *ab initio* calculations implemented in the CASTEP package through DFT.[41] The Heyd−Scuseria−Ernzerhof (HSE) hybrid function[42,43] was adopted to calculate the exchange−correlation potential, with an energy cutoff of 900 and 650 eV for $K_2FeGe_3S_8$ and $K_2CdGe_3S_8$, respectively. The numerical integration of the Brillouin zone was performed using a Monkhorst−Pack *k*-point sampling. The *k*-point separation for each material was set as 0.04 $Å^{-1}$. The geometry optimizations were applied prior to property calculations. Norm-conserving pseudopotentials were employed. The local-density approximation + *U* approach (where *U* is the Hubbard energy) is adopted to deal with strongly correlated compounds $K_2FeGe_3S_8$.

RESULTS AND DISCUSSION

Crystal Structure. $K_2CdGe_3S_8$ is isostructural to $K_2CdGe_3Se_8$, which both crystallize in the $K_2FeGe_3S_8$ structure type.[30] Other known isostructural compounds discovered recently are $K_2ZnSn_3Se_8$,[26] $K_2ZnGe_3S_8$,[33] and $Rb_2MnSn_3Se_8$,[25] which exhibit promising nonlinear optical properties. The selected structure refinement parameters and crystal data for $K_2CdGe_3Ch_8$ (Ch = S, Se) are summarized in Table S1. The refined atomic coordinates and selected important interatomic distances of $K_2CdGe_3Ch_8$ (Ch = S, Se) are summarized in Tables S2 and S3, respectively. Many previous studies have summarized the crystal structure of $II_2II_1IV_3Ch_8$ (II = K, Rb, Cs; II = Mn, Co, Fe, Zn, Cd; IV = Ge, Sn; and Ch = S, Se).[25−38] $K_2CdGe_3Ch_8$ (Ch = S, Se) are the newest members of the $II_2II_1IV_3Ch_8$ family. To simplify the discussion, $K_2CdGe_3S_8$ was selected to present the crystal structure of $K_2CdGe_3Ch_8$ (Ch = S, Se).

$K_2CdGe_3S_8$ forms in the noncentrosymmetric monoclinic space group $P2_1$ (no. 4) with unit cell parameters of a = 7.31139(10) Å, b = 12.05817(18) Å, and c = 16.9274(2) Å and β = 95.3987(12)°. The Wyckoff sequence of $K_2CdGe_3S_8$ is a^{28} with Pearson symbol *mP*56. Four distinct K atoms, two distinct Cd atoms, six distinct Ge atoms, and 16 distinct S atoms exist in the asymmetric unit cell of $K_2CdGe_3S_8$ with full occupancy. The crystal structure of $K_2CdGe_3S_8$ is summarized in Figure 1. $K_2CdGe_3S_8$ is constructed by neutral $[K_2CdGe_3S_8]$ slabs, as shown in Figure 1a. Each $[K_2CdGe_3S_8]$ slab is built by $[CdGe_3S_8]^{2-}$ anionic layers sandwiched by K^+ cations. The two-dimensional $[CdGe_3S_8]$ layers are constructed by one-dimensional $[CdGeS_6]$ chains interlinked by $[Ge_2S_6]$ units, which are presented in Figure 1b. The one-dimensional $[CdGeS_6]$ chain (Figure 1c) is formed by $[GeS_4]$ tetrahedra sharing vertices with $[CdS_4]$ tetrahedra. The $[Ge_2S_6]$ units (Figure 1d) are constructed by two $[GeS_4]$ tetrahedra sharing one edge.

The Ge−S bond distances in $K_2CdGe_3S_8$ fall into the range of 2.160(1)−2.261(1) Å, which are comparable to many germanium-sulfides such as $K_2FeGe_3S_8$ (2.181−2.239 Å),[30] $KBiGeS_4$ (2.181−2.239 Å),[44] $Cs_4GeP_4S_{12}$ (2.209−2.232 Å),[45] $K_2ZnGe_3S_8$ (2.148−2.285 Å),[33] $KLaGeS_4$ (2.175−2.220 Å),[46] $K_2MnGe_3S_8$ (2.125−2.288 Å),[32] $Na_5AgGe_2S_7$ (2.189−2.247 Å),[47] $La_4Ge_3S_{12}$ [2.196(7)−2.241(7) Å],[48] $Ba_6(Cu_{1.9}Mg_{1.1})Ge_4S_{16}$ [2.174(8)−2.227(5) Å],[49] and so forth. The Cd−S bond distances within $[CdS_4]$ tetrahedra of $K_2CdGe_3S_8$ are 2.486(5)−2.537(5) Å, which agree well with many cadmium-sulfides such as $KCd_4Ga_5S_{12}$ (2.335−2.429 Å),[50,51] K_2AuCdS_4 (2.597 Å),[52] $K_2Cd_3S_4$ (2.473−2.640 Å),[53] and so forth.

Another compound worthy to mention here is $K_2FeGe_3S_8$,[30] which is isostructural to $K_2CdGe_3Ch_8$ (Ch = S, Se). $K_2FeGe_3S_8$ exhibits much weaker SHG response than $K_2CdGe_3Ch_8$ (Ch = S, Se) (*vide infra*). The Ge−S interactions for $K_2FeGe_3S_8$ are close to $K_2CdGe_3S_8$ of 2.149(1)−2.280(1) and 2.146(5)−2.291(5) Å, respectively. The K−S interactions for $K_2FeGe_3S_8$ fall into the range of 3.131(4)−3.762(4) Å, which are comparable to the K−S interactions within $K_2CdGe_3S_8$ of 3.163(7)−3.709(8) Å. The large divalent Cd^{2+} in $K_2CdGe_3S_8$ results in enlarged Cd−S distances of 2.486(5)−2.537(5) Å, which is longer than Fe−S interactions within $K_2FeGe_3S_8$ of 2.332(3)−2.374(4) Å. The structural comparison between $K_2FeGe_3S_8$ and $K_2CdGe_3S_8$ is summarized in Table 1. $K_2CdGe_3S_8$ is isostructural to $K_2FeGe_3S_8$ with comparable Ge−S distances and K−S distances.

Table 1. Structural Comparison between $K_2FeGe_3S_8$ and $K_2CdGe_3S_8$

	$K_2FeGe_3S_8$[30]	$K_2CdGe_3S_8$ this work
unit cell dimensions	a = 7.1089(5) Å	a = 7.31139(10) Å
	b = 11.8823(8) Å	b = 12.05817(18) Å
	c = 16.7588(11) Å	c = 16.9274(2) Å
	β = 92.647(3)°	β = 95.3987(12)°
unit cell volume	1406.23(17) $Å^3$	1485.73(3) $Å^3$
K−S distances	3.131(4)−3.762(4) Å	3.163(7)−3.709(8) Å
Ge−S distances	2.149(1)−2.280(1) Å	2.146(5)−2.291(5) Å
T−S distances (T = Fe, Cd)	2.332(3)−2.374(4) Å	2.486(5)−2.537(5) Å

Linear and Nonlinear Optical Properties. Even though $K_2FeGe_3S_8$ is isostructural to $K_2CdGe_3S_8$, $K_2CdGe_3S_8$ owns superior SHG response compared to $K_2FeGe_3S_8$: 4.5× $AgGaS_2$, and 0.25× $AgGaS_2$, respectively (for samples of particle size of 38−55 μm) (Figure 2b). Notably, the SHG intensity of $K_2CdGe_3S_8$ is 18× $K_2FeGe_3S_8$. For samples of particle size of 200−250 μm, the SHG intensity of $K_2CdGe_3S_8$ is 77× $K_2FeGe_3S_8$. A summary of the optical properties of the $II_2II_1IV_3Ch_8$ family is listed in Table S4. As shown in Table S4, the SHG of many compounds within the $II_2II_1IV_3Ch_8$ family was not measured. $K_2CdGe_3S_8$ possesses a better SHG response than compounds previously characterized in the $II_2II_1IV_3Ch_8$ family.[25−38] The cation substitution within the $II_2II_1IV_3Ch_8$ family greatly affects their crystal structures and nonlinear optical properties.[25−38] The SHG response of $K_2CdGe_3Ch_8$ (Ch = S, Se) is presented in Figure 2a. $K_2CdGe_3S_8$ and $K_2CdGe_3Se_8$ were revealed as type-I phase-matching materials, where the SHG intensity increases as particle size increases. The phase-matching capability of $K_2CdGe_3Ch_8$ (Ch = S, Se) was supported by calculated birefringence results (Figures S6 and S7). $K_2CdGe_3Ch_8$ (Ch = S, Se) crystals exhibit moderate birefringence. As shown in Figures S6 and S7, $K_2CdGe_3Se_8$ exhibits larger birefringence than $K_2CdGe_3S_8$. For an incident laser of 2 μm, Δn is 0.22 and 0.26 for $K_2CdGe_3S_8$ and $K_2CdGe_3Se_8$, respectively. For samples of particle size of 200−250 μm, the SHG intensity is 2.1× $AgGaS_2$ and 1.3× $AgGaS_2$ for $K_2CdGe_3S_8$ and $K_2CdGe_3Se_8$, respectively. $K_2CdGe_3S_8$ exhibits better SHG response than $K_2CdGe_3Se_8$. Generally, the SHG response is inversely proportional to the band gaps.[54,55] Please note that many factors such as the strong absorption coefficient and

https://doi.org/10.1021/acs.inorgchem.2c03852
Inorg. Chem. 2023, 62, 574−582

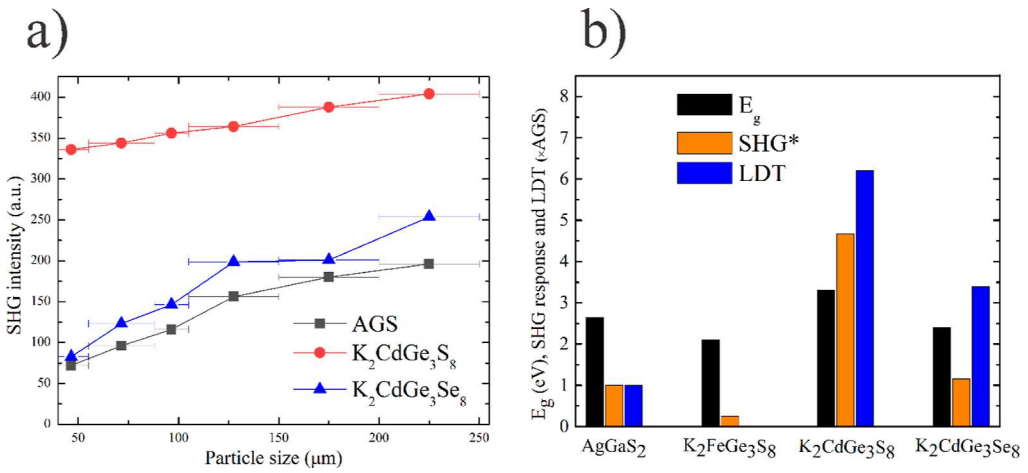

Figure 2. (a) SHG intensity of $K_2CdGe_3Ch_8$ (Ch = S, Se) compared with $AgGaS_2$. (b) Comparison of band gaps, LDTs, and SHG intensity between $AgGaS_2$, $K_2FeGe_3S_8$, $K_2CdGe_3S_8$, and $K_2CdGe_3Se_8$. *The SHG intensity is based on samples of particle size of 38−55 μm.

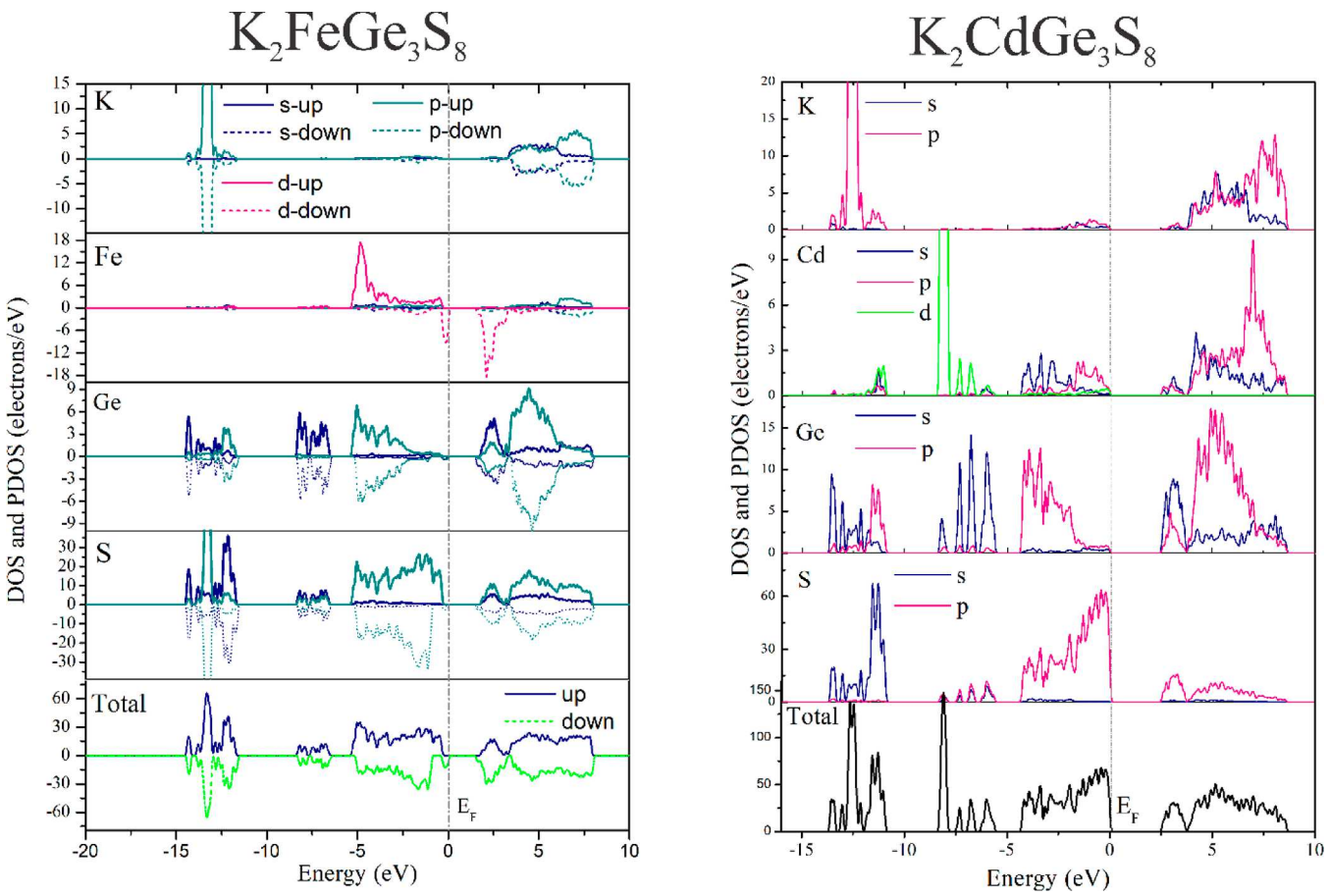

Figure 3. Calculated DOS of $K_2FeGe_3S_8$ (left) and $K_2CdGe_3S_8$ (right). Both spin-up and spin-down states are presented for $K_2FeGe_3S_8$ (left).

easily clustered particles of selenides may affect the SHG measurement results.[56] Isostructural sulfides and selenides might exhibit different NLO optical properties. As summarized in Table S5, some selected sulfides exhibit better SHG response than the isostructural selenides.[57−62] The band gaps of $K_2CdGe_3Ch_8$ (Ch = S, Se) were estimated by UV−vis methods (Figures S8−S10). $K_2TGe_3S_8$ (T = Fe, Cd) was predicted to be an indirect band gap semiconductor (*vide infra*). The indirect band gaps for $K_2CdGe_3S_8$ and $K_2CdGe_3Se_8$ are 3.3(1) and 2.3(1) eV, respectively, which are comparable to $AgGaS_2$ at 2.6 eV. Due to the large band gap, $K_2CdGe_3S_8$ owns an extraordinary LDTs of 6.2(1)× $AgGaS_2$ (Figure 2b). $K_2CdGe_3Se_8$ has a moderate-high LDTs of 3.4(1)× $AgGaS_2$. Many factors, such as band gap, absorption coefficient, thermal conductivity, and thermal expansion coefficient, contribute to the LDTs of solids.[49] As summarized in Table S6, many small band gap selenides exhibit high LDTs and high SHG.[63−71] $K_2CdGe_3S_8$ is a promising candidate for infrared NLO material, which combines suitable band gap, good stability, high SHG intensity, high LDTs, and type-I phase-matching

https://doi.org/10.1021/acs.inorgchem.2c03852
Inorg. Chem. 2023, 62, 574−582

behavior. One interesting question raised here would be why $K_2CdGe_3S_8$ shows a much better SHG response than $K_2FeGe_3S_8$ regardless of their isostructural nature. Understanding the origin of high SHG response is critical for designing emerging NLO materials.[54,55] What are the chemical reasons for the enhancement of the SHG response of $K_2CdGe_3S_8$ *versus* $K_2FeGe_3S_8$?

DFT Calculations. To elucidate the origin of the superior SHG intensity of $K_2CdGe_3S_8$, electronic structures were evaluated (Figure 3 right). The electronic structure of $K_2FeGe_3S_8$ was also calculated and is presented in Figure 3 (left) with the presence of both spin-up and spin-down models. The top of the valance bands of $K_2FeGe_3S_8$ is mainly contributed by Fe 3d orbitals, Ge 4p orbitals, and S 3p orbitals. The 3d orbitals of Fe show a strong spin-polarized electronic configuration that indicates magnetic properties of $K_2FeGe_3S_8$, which were experimentally verified.[30] The bottom of the conduction bands is dominantly contributed by orbitals from Fe atoms (3d orbitals) and S atoms (3s and 3p orbitals) and orbitals from Ge atoms (4s and 4p orbitals), while the K orbitals have minimal contributions. The optical properties of $K_2FeGe_3S_8$ are mainly controlled by Ge−S interactions and Fe−S interactions. For $K_2CdGe_3S_8$, the top of the valance band is mainly contributed by S 3p orbitals together with significant contributions from Ge 4p orbitals and Cd 5p and 5d orbitals. The bottom of the conduction band within $K_2CdGe_3S_8$ is dominantly contributed by S 3p orbitals, Ge 4s and Ge 4p orbitals, and certain contributions from Cd 5p and Cd 5s orbitals. The Cd 5d orbitals are mainly located at the interval of −6 to −8 eV. The orbitals from K atoms have negligible contributions to the top of valance bands and the bottom of conduction bands. We can expect that the Cd−S interactions and Ge−S interactions will significantly affect the optical properties of $K_2CdGe_3S_8$, which is confirmed by DFT calculations (*vide infra*).

The semiconducting nature of $K_2FeGe_3S_8$ and $K_2CdGe_3S_8$ was confirmed by electronic calculations (Figures 3, S11, and S12). The calculated band gaps for $K_2FeGe_3S_8$ and $K_2CdGe_3S_8$ are 1.49 and 2.54 eV, respectively (Figures S11 and S12). Both $K_2FeGe_3S_8$ and $K_2CdGe_3S_8$ are predicted to be indirect band gap semiconductors. The experimentally estimated band gaps for $K_2FeGe_3S_8$ and $K_2CdGe_3S_8$ are 1.7(1) and 3.3(1) eV, respectively. The significant discrepancy between the theory-calculated band gaps and the experimentally measured results originates from the DFT calculations intrinsically underestimating band gaps of solids.[55] The semiconducting nature of $K_2FeGe_3S_8$ and $K_2CdGe_3S_8$ is also supported by the charge-balanced formulas $[K^+]_2[Fe^{2+}][Ge^{4+}]_3[S^{2-}]_8$ ($K_2FeGe_3S_8$) and $[K^+]_2[Cd^{2+}][Ge^{4+}]_3[S^{2-}]_8$ ($K_2CdGe_3S_8$) *via* assigning a formal charge of 1+ to the K atoms, 2+ to the Fe/Cd atoms, 4+ to the Ge atoms, and 2− to the S atoms. The divalent nature of the Fe atom within $K_2FeGe_3S_8$ was verified by magnetic measurements.[30]

The nonlinear optical properties of $K_2FeGe_3S_8$ and $K_2CdGe_3S_8$ were evaluated by DFT calculations (Figure 4 and Table 2). The calculated effective SHG response of $K_2CdGe_3S_8$ is 2.27 pm V^{-1}. As presented in Table 2, $K_2CdGe_3S_8$ exhibits a much stronger SHG response than $K_2FeGe_3S_8$, which roughly agrees well with our experimental observations.

The SHG intensity simulations, both the VE occupied states and VE unoccupied states presented in Figure 4, elucidate that the second harmonic response in the occupied states is mainly

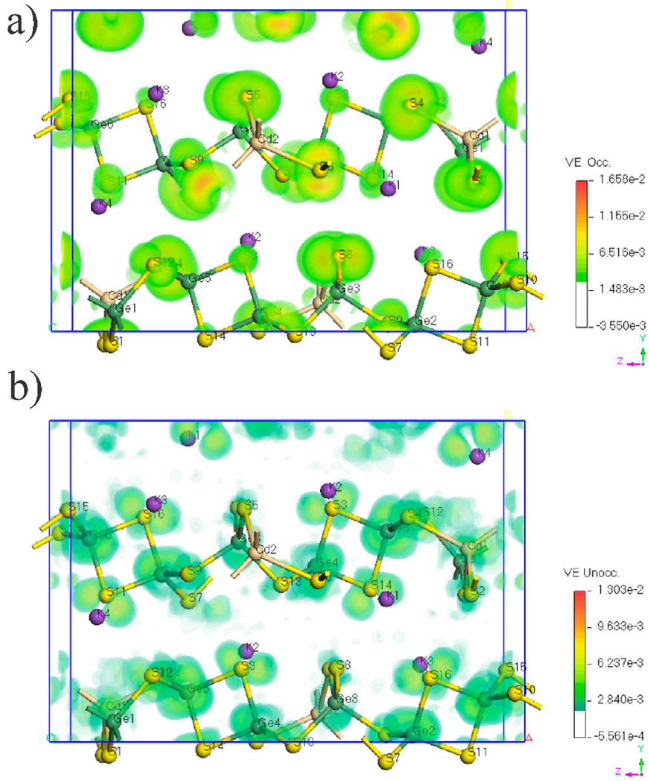

Figure 4. (a) SHG density of virtual electron (VE) occupied states (VE_{occ}) and (b) VE unoccupied states (VE_{unocc}) of $K_2CdGe_3S_8$.

Table 2. Calculated Second-Order Nonlinear Susceptibility χ^{abc} for $K_2FeGe_3S_8$ and $K_2CdGe_3S_8$

	$K_2FeGe_3S_8$	$K_2CdGe_3S_8$
χ^{112}/(pm V^{-1})	−0.068	0.965
χ^{123}/(pm V^{-1})	0.463	−1.174
χ^{222}/(pm V^{-1})	−5.228	−8.607
χ^{233}/(pm V^{-1})	0.009	−1.076

contributed by S atoms for $K_2CdGe_3S_8$. For the unoccupied states, there are significant contributions from Ge-, Cd-, and S-atoms. These simulations agree well with our electronic structure calculations, where the Cd−S and Ge−S interactions are proposed to dominate the optical properties of $K_2CdGe_3S_8$. Through a combination of property measurements, electronic structure studies, and DFT calculations, the enhancement of SHG intensity in $K_2CdGe_3S_8$ compared to $K_2FeGe_3S_8$ mainly originates from the different characteristics between Cd and Fe, including electron configuration, electronegativity, ionic radius, and so forth. The strongly spin-polarized electronic structure of Fe within $K_2FeGe_3S_8$ does not show advantages to SHG effects even though it has a smaller band gap compared with $K_2CdGe_3S_8$. A similar observation was also found within $K_2ZnGe_3S_8$,[33] where the d^{10}-Zn replacement of d^6-Fe resulted in a better SHG response ($K_2ZnGe_3S_8$ = 3.6 × $K_2FeGe_3S_8$). When d^5-Mn^{2+} is replacing d^6-Fe^{2+}, $K_2MnGe_3S_8$ exhibits a comparable SHG response with $K_2FeGe_3S_8$.[32] Please note here that the $K_2MnGe_3S_8$ crystallizes in the same space group ($P2_1$) as $K_2FeGe_3S_8$ with the *c*-axis doubled.[32] The highly chemically flexible $II_2II_1IV_3Ch_8$ family provides a good platform to uncover emerging NLO materials.[25−38] Our previous study about $K_2TGe_3S_8$ (T = Co, Fe) reveals the importance of $[CoS_4]$ and $[FeS_4]$ tetrahedra affecting the crystal structure.[30]

https://doi.org/10.1021/acs.inorgchem.2c03852
Inorg. Chem. 2023, 62, 574−582

In this work, the fully occupied d^{10} transition metal Cd is demonstrated to play an important role in enhancing the SHG response compared to d^6-Fe in $K_2TGe_3Ch_8$ (T = Fe, Cd; Ch = S, Se). The origin of high SHG response is crucial to NLO research and a comprehensive question. Trying to eliminate the possible contribution from crystal quality and measurement processes, high-quality crystals of $K_2TGe_3Ch_8$ (T = Fe, Cd and Ch = S, Se) were measured under identical conditions. One hypothesis would be the distortion degree of $[CdS_4]$ and $[FeS_4]$ tetrahedra, which play a key role in enhancing SHG response. From electronic structure analysis, Fe atoms contribute about 3 electrons/eV to the total of ∼30 electrons/eV around the Fermi level within $K_2FeGe_3S_8$. The Cd atoms contribute around 3 electrons/eV to the total of ∼60 electrons/eV around the Fermi level within $K_2CdGe_3S_8$. Both the Fe atoms and Cd atoms have a limited contribution to the optical properties of $K_2FeGe_3S_8$ and $K_2CdGe_3S_8$, respectively. Another point worth mentioning here would be the distortion degree of $[CdS_4]$ and $[FeS_4]$ tetrahedra. For a tetrahedral $[MX_4]$, the distortion degree can be determined by the following formula: $\Delta d = \left(\frac{1}{4}\right)\sum\left[\frac{d_i - d}{d}\right]$, where d_i represents the length of four individual M−X bonds and d is the average length of the four bonds.[72−81] To better estimate the distortion degree, we employed a modified calculation equation: $\Delta d = \left(\frac{1}{4}\right)\sum\left|\left[\frac{d_i - d}{d}\right]\right|$. The detailed distortion degree results for all tetrahedrons of $K_2TGe_3Ch_8$ (T = Fe, Cd; Ch = S, Se) are summarized in Table S7. Overall, $[GeCh_4]$ (Ch = S, Se) tetrahedra own a higher degree of distortion than $[TCh_4]$ (T = Fe, Cd and Ch = S, Se) tetrahedra. The distortion degrees for the $[Fe1S_4]$ tetrahedra and the $[Fe2S_4]$ tetrahedra are 4.52×10^{-3} and 4.70×10^{-3}, respectively, within $K_2FeGe_3S_8$. The distortion degrees for the $[Cd1S_4]$ tetrahedra and the $[Cd2S_4]$ tetrahedra are 3.07×10^{-3} and 6.37×10^{-3}, respectively, within $K_2CdGe_3S_8$. The $[Cd2S_4]$ tetrahedron within $K_2CdGe_3S_8$ exhibits a much higher degree of distortion than the $[FeS_4]$ tetrahedra within $K_2FeGe_3S_8$. The averaged distortion degrees of $[GeS_4]$ tetrahedra are 18.2×10^{-3} and 16.5×10^{-3} for $K_2CdGe_3S_8$ and $K_2FeGe_3S_8$, respectively. The highly distorted $[Cd2S_4]$ tetrahedron with a bigger volume coupled with the distorted $[GeS_4]$ tetrahedron within $K_2CdGe_3S_8$ may play an important role in enhancing the SHG response.[30] When comparing $K_2CdGe_3S_8$ with $K_2CdGe_3Se_8$, $K_2CdGe_3S_8$ shows better SHG response than $K_2CdGe_3Se_8$. The averaged degree of distortion of $[GeS_4]$ and $[GeSe_4]$ tetrahedra is 18.2×10^{-3} and 18.3×10^{-3} for $K_2CdGe_3S_8$ and $K_2CdGe_3Se_8$, respectively. The $[CdS_4]$ tetrahedron within $K_2CdGe_3S_8$ possesses a higher degree of distortion than the $[CdSe_4]$ tetrahedron with $K_2CdGe_3Se_8$ (Table S7), which may play a role in enhancing SHG response of $K_2CdGe_3S_8$ compared to $K_2CdGe_3Se_8$. More work such as growing high-quality large single crystals to accurately determine the SHG coefficients is required to elucidate the properties difference between $K_2FeGe_3S_8$, $K_2CdGe_3S_8$, and $K_2CdGe_3S_8$ and is ongoing.

CONCLUSIONS

Two promising infrared nonlinear optical materials, $K_2CdGe_3S_8$ and $K_2CdGe_3Se_8$, were synthesized *via* conventional high temperature solid-state reactions. $K_2CdGe_3S_8$ and $K_2CdGe_3Se_8$ are new members of the $II_2II_1IV_3Ch_8$ family. Nonlinear optical property measurements revealed that $K_2CdGe_3S_8$ possesses a much higher SHG response than $K_2FeGe_3S_8$, 4.5× $AgGaS_2$, and 0.25× $AgGaS_2$, respectively (samples of particle sizes of 38−55 μm). Notably, $K_2CdGe_3S_8$ is 18× $K_2FeGe_3S_8$. The origin of superior nonlinear optical properties of $K_2CdGe_3S_8$ is understood by optical property measurements, electronic structure calculations, and DFT calculations. The chemical characteristic difference between Cd and Fe including fully occupied d^{10} electron configuration, electronegativity, ionic radius, and so forth, which results in highly distorted and larger volume $[CdS_4]$ tetrahedra, responds to the optical property differences. $K_2CdGe_3S_8$ was demonstrated as a promising nonlinear optical material with type-I phase-matching behavior, good air stability, high SHG response (2.1× $AgGaS_2$, samples of particle sizes of 200−250 μm), and high LDTs (6.2× $AgGaS_2$). This research verified that elements with d−d transitions should be avoided for NLO applications.

ASSOCIATED CONTENT

Supporting Information

The Supporting Information is available free of charge at https://pubs.acs.org/doi/10.1021/acs.inorgchem.2c03852.

Refined crystallographic data, microscopy photograph of crystals, laboratory X-ray diffraction and 11-BM diffraction results, UV−vis results and Tauc plot, HSE band structures, and calculated birefringence (PDF)

Accession Codes

CCDC 2177915−2177916 contain the supplementary crystallographic data for this paper. These data can be obtained free of charge via www.ccdc.cam.ac.uk/data_request/cif, or by emailing data_request@ccdc.cam.ac.uk, or by contacting The Cambridge Crystallographic Data Centre, 12 Union Road, Cambridge CB2 1EZ, UK; fax: +44 1223 336033.

AUTHOR INFORMATION

Corresponding Authors

Bingbing Zhang − *Key Laboratory of Analytical Science and Technology of Hebei Province, College of Chemistry and Environmental Science, Hebei University, Baoding 071002, China*; Email: zhangbb@hbu.edu.cn

Jian Wang − *Department of Chemistry and Biochemistry, Wichita State University, Wichita, Kansas 67260, United States*; orcid.org/0000-0003-1326-4470; Email: jian.wang@wichita.edu

Authors

Bingheng Ji − *Department of Chemistry and Biochemistry, Wichita State University, Wichita, Kansas 67260, United States*

Fei Wang − *Department of Chemistry, Missouri State University, Springfield, Missouri 65897, United States*; orcid.org/0000-0001-6957-1360

Kui Wu − *Key Laboratory of Analytical Science and Technology of Hebei Province, College of Chemistry and Environmental Science, Hebei University, Baoding 071002, China*; orcid.org/0000-0001-8242-4613

Complete contact information is available at: https://pubs.acs.org/10.1021/acs.inorgchem.2c03852

Notes

The authors declare no competing financial interest.

https://doi.org/10.1021/acs.inorgchem.2c03852
Inorg. Chem. 2023, 62, 574−582

■ ACKNOWLEDGMENTS

This research is supported by start-up funds from the Wichita State University. Use of the Advanced Photon Source, an Office of Science User Facility operated for the U.S. Department of Energy (DOE) Office of Science by Argonne National Laboratory, was supported by the U.S. DOE under contract no. DE-AC02-06CH11357.

■ REFERENCES

(1) Chen, C.; Wu, B.; Jiang, A.; You, G. A new-type ultraviolet SHG crystal—β-BaB_2O_4. *Sci. Sin., Ser. B* **1985**, *28*, 235−243.
(2) Chen, C.; Wu, Y.; Jiang, A.; Wu, B.; You, G.; Li, R.; Lin, S. New nonlinear-optical crystal: LiB_3O_5. *J. Opt. Soc. Am. B* **1989**, *6*, 616−621.
(3) Weis, R. S.; Gaylord, T. K. Lithium niobate: Summary of physical properties and crystal structure. *Appl. Phys. A: Solids Surf.* **1985**, *37*, 191−203.
(4) Dmitriev, V. G.; Gurzadyan, G. G.; Nikogosyan, D. N.*Handbook of Nonlinear Optical Crystals*, 3rd ed.; Springer-Verlag: Berlin, Heidelberg, Germany, 1999.
(5) Driscoll, T. A.; Perkins, P. E.; Hoffman, H. J.; Stone, R. E. Efficient Second-Harmonic Generation in KTP Crystals. *J. Opt. Soc. Am. B* **1986**, *3*, 683.
(6) Chen, C.; Wang, Y.; Wu, B.; Wu, K.; Zeng, W.; Yu, L. Design and Synthesis of an Ultraviolet-Transparent Nonlinear Optical Crystal $Sr_2Be_2B_2O_7$. *Nature* **1995**, *373*, 322−324.
(7) Kang, L.; Zhou, M.; Yao, J.; Lin, Z.; Wu, Y.; Chen, C. Metal Thiophosphates with Good Mid-Infrared Nonlinear Optical Performances: A First-Principles Prediction and Analysis. *J. Am. Chem. Soc.* **2015**, *137*, 13049−13059.
(8) Zhang, H.; Zhang, M.; Pan, S.; Dong, X.; Yang, Z.; Hou, X.; Wang, Z.; Chang, K. B.; Poeppelmeier, K. R. $Pb_{17}O_8Cl_{18}$: A Promising IR Nonlinear Optical Material with Large Laser Damage Threshold Synthesized in an Open System. *J. Am. Chem. Soc.* **2015**, *137*, 8360−8363.
(9) Yu, H.; Young, J.; Wu, H.; Zhang, W.; Rondinelli, J. M.; Halasyamani, P. S. Electronic, Crystal Chemistry, and Nonlinear Optical Property Relationships in the Dugganite $A_3B_3CD_2O_{14}$ Family. *J. Am. Chem. Soc.* **2016**, *138*, 4984−4989.
(10) Chung, I.; Kanatzidis, M. G. Metal Chalcogenides: A Rich Source of Nonlinear Optical Materials. *Chem. Mater.* **2014**, *26*, 849−869.
(11) Bera, T. K.; Jang, J. I.; Ketterson, J. B.; Kanatzidis, M. G. Strong Second Harmonic Generation from the Tantalum Thioarsenates $A_3Ta_2AsS_{11}$ (A = K and Rb). *J. Am. Chem. Soc.* **2009**, *131*, 75−77.
(12) Liang, F.; Kang, L.; Lin, Z.; Wu, Y. Mid-Infrared Nonlinear Optical Materials Based on Metal Chalcogenides: Structure−Property Relationship. *Cryst. Growth Des.* **2017**, *17*, 2254−2289.
(13) Abudurusuli, A.; Li, J.; Pan, S. A review on the recently developed promising infrared nonlinear optical materials. *Dalton Trans.* **2021**, *50*, 3155−3160.
(14) Wei, Q.; He, C.; Wang, K.; Duan, X.-F.; An, X.-T.; Li, J.-H.; Wang, G.-M. $Sb_6O_7(SO_4)_2$: A Promising Ultraviolet Nonlinear Optical Material with an Enhanced Second-Harmonic-Generation Response Activated by Sb^{III} Lone-Pair Stereoactivity. *Chem.—Eur. J.* **2021**, *27*, 5880−5884.
(15) Luo, M.; Liang, F.; Hao, X.; Lin, D.; Li, B.; Lin, Z.; Ye, N. Rational Design of the Nonlinear Optical Response in a Tin Iodate Fluoride $Sn(IO_3)_2F_2$. *Chem. Mater.* **2020**, *32*, 2615−2620.
(16) Yin, R.; Hu, C.; Lei, B.-H.; Pan, S.; Yang, Z. Lone Pair Effects on Ternary Infrared Nonlinear Optical Materials. *Phys. Chem. Chem. Phys.* **2019**, *21*, 5142−5147.
(17) Chang, H.-Y.; Kim, S.-H.; Halasyamani, P. S.; Ok, K. M. Alignment of Lone Pairs in a New Polar Material: Synthesis, Characterization, and Functional Properties of $Li_2Ti(IO_3)_6$. *J. Am. Chem. Soc.* **2009**, *131*, 2426−2427.
(18) Cai, W.; Jing, Q.; Zhang, J. Lone Pair Electron Effect Induced Differences in Linear and Nonlinear Optical Properties of Bismuth Borates. *New J. Chem.* **2020**, *44*, 1228−1235.
(19) Gong, P.; Liu, X.; Kang, L.; Lin, Z. Inorganic Planar π-Conjugated Groups in Nonlinear Optical Crystals: Review and Outlook. *Inorg. Chem. Front.* **2020**, *7*, 839−852.
(20) Liu, Y.; Shen, Y.; Zhao, S.; Luo, J. Structure-Property Relationship in Nonlinear Optical Materials with π-Conjugated CO_3 Triangles. *Coord. Chem. Rev.* **2020**, *407*, 213152.
(21) Kang, L.; Liang, F.; Jiang, X.; Lin, Z.; Chen, C. First-Principles Design and Simulations Promote the Development of Nonlinear Optical Crystals. *Acc. Chem. Res.* **2020**, *53*, 209−217.
(22) Zhang, W.; Yu, H.; Wu, H.; Halasyamani, P. S. Phase-Matching in Nonlinear Optical Compounds: A Materials Perspective. *Chem. Mater.* **2017**, *29*, 2655−2668.
(23) Liu, H.; Zhang, B.; Wang, Y. Second-Order Nonlinear Optical Materials with a Benzene-like Conjugated π System. *Chem. Commun.* **2020**, *56*, 13689−13701.
(24) Chu, Y.; Li, G.; Su, X.; Wu, K.; Pan, S. A Review on the Development of Infrared Nonlinear Optical Materials with Triangular Anionic Groups. *J. Solid State Chem.* **2019**, *271*, 266−272.
(25) Hu, X.-N.; Xiong, L.; Wu, L.-M. Six New Members of the $A_2MIIMIV_3Q_8$ Family and Their Structural Relationship. *Cryst. Growth Des.* **2018**, *18*, 3124−3131.
(26) Zhou, M.; Jiang, X.; Yang, Y.; Guo, Y.; Lin, Z.; Yao, J.; Wu, Y. $K_2ZnSn_3Se_8$: A Non-Centrosymmetric Zinc Selenidostannate(IV) Featuring Interesting Covalently Bonded $[ZnSn_3Se_8]^{2-}$ Layer and Exhibiting Intriguing Second Harmonic Generation Activity. *Chem.—Asian J.* **2017**, *12*, 1282−1285.
(27) Fard, Z. H.; Kanatzidis, M. G. Phase-Change Materials Exhibiting Tristability: Interconverting Forms of Crystalline α-, β-, and Glassy $K_2ZnSn_3S_8$. *Inorg. Chem.* **2012**, *51*, 7963−7965.
(28) Morris, C. D.; Li, H.; Jin, H.; Malliakas, C. D.; Peters, J. A.; Trikalitis, P. N.; Freeman, A. J.; Wessels, B. W.; Kanatzidis, M. G. $Cs_2M^{II}M^{IV}{}_3Q_8$(Q = S, Se, Te): An Extensive Family of Layered Semiconductors with Diverse Band Gaps. *Chem. Mater.* **2013**, *25*, 3344−3356.
(29) Lin, H.; Wei, W.-B.; Chen, H.; Wu, X.-T.; Zhu, Q.-L. Rational Design of Infrared Nonlinear Optical Chalcogenides by Chemical Substitution. *Coord. Chem. Rev.* **2020**, *406*, 213150.
(30) Ji, B.; Pandey, K.; Harmer, C. P.; Wang, F.; Wu, K.; Hu, J.; Wang, J. Centrosymmetric or Noncentrosymmetric? Transition Metals Talking in $K_2TGe_3S_8$(T = Co, Fe). *Inorg. Chem.* **2021**, *60*, 10603−10613.
(31) Feng, K.; Wang, W.; He, R.; Kang, L.; Yin, W.; Lin, Z.; Yao, J.; Shi, Y.; Wu, Y. $K_2FeGe_3Se_8$: A New Antiferromagnetic Iron Selenide. *Inorg. Chem.* **2013**, *52*, 2022−2028.
(32) Li, Z.; Jiang, X.; Yi, C.; Zhou, M.; Guo, Y.; Luo, X.; Lin, Z.; Wu, Y.; Shi, Y.; Yao, J. $K_2MnGe_3S_8$: A New Multifunctional Semiconductor Featuring $[MnGe_3S_8]^{2-}$ Layers and Demonstrating Interesting Nonlinear Optical Response and Antiferromagnetic Properties. *J. Mater. Chem. C* **2018**, *6*, 10042−10049.
(33) Luo, X.; Liang, F.; Zhou, M.; Guo, Y.; Li, Z.; Lin, Z.; Yao, J.; Wu, Y. $K_2ZnGe_3S_8$: A Congruent-Melting Infrared Nonlinear-Optical Material with a Large Band Gap. *Inorg. Chem.* **2018**, *57*, 9446−9452.
(34) Hahn, S.-I.; Kim, P.; Yun, H. Synthesis and Crystal Structure of the New Selenogermanate, $Cs_2CdGe_3Se_8$. *Bull. Korean Chem. Soc.* **2013**, *34*, 1250−1252.
(35) Gao, L.; Yang, Y.; Zhang, B.; Wu, X.; Wu, K. Triclinic Layered $A_2ZnSi_3S_8$ (A = Rb and Cs) with Large Optical Anisotropy and Systematic Research on the Inherent Structure-Performance Relationship in the $A_2M^{IIB}M^{IV}{}_3Q_8$ Family. *Inorg. Chem.* **2021**, *60*, 12573−12579.
(36) Wang, W.; Cao, W.; Zhang, L.; Li, G.; Wu, Y.; Wen, S.; Mei, D. Rb2FeGe3S8 and Cs2FeGe3S8: New Layered Chalcogenides in A2MIIMIV3Q8 Family with Antiferromagnetic Property. *J. Solid State Chem.* **2022**, *313*, 123276.
(37) Li, X.; Li, C.; Gong, P.; Lin, Z.; Yao, J.; Wu, Y. Syntheses, Crystal Structures and Physical Properties of Three New Chalcogenides: $NaGaGe_3Se_8$, $K_3Ga_3Ge_7S_{20}$, and $K_3Ga_3Ge_7Se_{20}$. *Dalton Trans.* **2016**, *45*, 532−538.

https://doi.org/10.1021/acs.inorgchem.2c03852
Inorg. Chem. 2023, 62, 574−582

(38) Pogu, A.; Vidyasagar, K. Syntheses, Structural Variants and Characterization of A2ZnSn3S8 (A = Cs, Rb) and A2CdSn3S8 (A = Cs, Rb, K, Na) Compounds. *J. Solid State Chem.* **2020**, *291*, 121647.
(39) Agilent Technologies. *XRD Products; CrysAlis Pro*; Agilent Technologies, Inc, 2019.
(40) Kurtz, S. K.; Perry, T. T. A Powder Technique for the Evaluation of Nonlinear Optical Materials. *J. Appl. Phys.* **1968**, *39*, 3798.
(41) Pfrommer, B. G.; Côté, M.; Louie, S. G.; Cohen, M. L. Relaxation of Crystals with the Quasi-Newton Method. *J. Comput. Phys.* **1997**, *131*, 233−240.
(42) Heyd, J.; Scuseria, G. E.; Ernzerhof, M. Hybrid functionals based on a screened Coulomb potential. *J. Chem. Phys.* **2003**, *118*, 8207.
(43) Krukau, A. V.; Vydrov, O. A.; Izmaylov, A. F.; Scuseria, G. E. Influence of the exchange screening parameter on the performance of screened hybrid functionals. *J. Chem. Phys.* **2006**, *125*, 224106.
(44) Mei, D.; Lin, Z.; Bai, L.; Yao, J.; Fu, P.; Wu, Y. KBiMS4 (M=Si, Ge): Synthesis, Structure, and Electronic Structure. *J. Solid State Chem.* **2010**, *183*, 1640−1644.
(45) Morris, C. D.; Chung, I.; Park, S.; Harrison, C. M.; Clark, D. J.; Jang, J. I.; Kanatzidis, M. G. Molecular Germanium Selenophosphate Salts: Phase-Change Properties and Strong Second Harmonic Generation. *J. Am. Chem. Soc.* **2012**, *134*, 20733−20744.
(46) Wu, P.; Ibers, J. A. Synthesis and Structures of the Quaternary Chalcogenides of the Type $KLnMQ_4$ (Ln = La, Nd, Gd, Y; M = Si, Ge; Q = S, Se). *J. Solid State Chem.* **1993**, *107*, 347−355.
(47) Zhang, C.; Wang, K.-N.; Ji, M.; An, Y.-L. Mild Solvothermal Syntheses of Thioargentates A-Ag-S (A = K, Rb, Cs) and A-Ag-Ge-S (A = Na, Rb): Crucial Role of Excess Sulfur. *Inorg. Chem.* **2013**, *52*, 12367−12371.
(48) Cicirello, G.; Wu, K.; Zhang, B. B.; Wang, J. Applying Band Gap Engineering to Tune the Linear Optical and Nonlinear Optical Properties of Noncentrosymmetric Chalcogenides $La_4Ge_3Se_xS_{12-x}$ (x = 0, 2, 4, 6, 8, 10). *Inorg. Chem. Front.* **2021**, *8*, 4914−4923.
(49) Ji, B.; Wu, K.; Chen, Y.; Wang, F.; Rossini, A. J.; Zhang, B.; Wang, J. Ba6(CuxZy)Sn4S16 (Z = Mg, Mn, Zn, Cd, in, Bi, Sn): High Chemical Flexibility Resulting in Good Nonlinear-Optical Properties. *Inorg. Chem.* **2022**, *61*, 2640−2651.
(50) Lin, H.; Zhou, L.-J.; Chen, L. Sulfides with Strong Nonlinear Optical Activity and Thermochromism: $ACd_4Ga_5S_{12}$ (A = K, Rb, Cs). *Chem. Mater.* **2012**, *24*, 3406−3414.
(51) Schwer, H.; Keller, E.; Krämer, V. Crystal Structure and Twinning of $KCd_4Ga_5S_{12}$ and Some Isotypic $AB_4C_5X_{12}$ Compounds. *Z. Kristallogr.—Cryst. Mater.* **1993**, *204*, 203−214.
(52) Axtell, E. A., III; Kanatzidis, M. G. First Examples of Gold Thiocadmates: $A_2Au_2Cd_2S_4$ (A=Rb, Cs) and $K_2Au_4CdS_4$: Bright Photoluminescence from New Alkali Metal/Gold Thiocadmates. *Chemistry* **1998**, *4*, 2435−2441.
(53) Axtell, E. A.; Liao, J.-H.; Pikramenou, Z.; Kanatzidis, M. G. Dimensional reduction in II-VI materials: $A_2Cd_3Q_4$ (A = K, Q = S, Se, Te; A = Rb, Q = S, Se), novel ternary low-dimensional cadmium chalcogenides produced by incorporation of A2Q in CdQ. *Chemistry* **1996**, *2*, 656−666.
(54) Ji, B.; Sarkar, A.; Wu, K.; Swindle, A.; Wang, J. $A_2P_2S_6$ (A=Ba, Pb): A Good Platform to Study Polymorph Effect and Lone Pairs Effect to Form Acentric Structure. *Dalton Trans.* **2022**, *51*, 4522−4531.
(55) Nguyen, V.; Ji, B.; Wu, K.; Zhang, B.; Wang, J. Unprecedented Mid-Infrared Nonlinear Optical Materials Achieved by Crystal Structure Engineering, a Case Study of $(KX)P_2S_6$(X=Sb, Bi, Ba). *Chem. Sci.* **2022**, *13*, 2640−2648.
(56) Clark, D. J.; Zhang, J.-H.; Craig, A. J.; Weiland, A.; Brant, J. A.; Cho, J. B.; Kim, Y. S.; Jang, J. I.; Aitken, J. A. The Kurtz-Perry powder technique revisited: A case study on the importance of reference quality and broadband nonlinear optical measurements using $LiInSe_2$. *J. Alloys Compd.* **2022**, *917*, 165381.
(57) Lekse, J. W.; Moreau, M. A.; McNerny, K. L.; Yeon, J.; Halasyamani, P. S.; Aitken, J. A. Second-Harmonic Generation and Crystal Structure of the Diamond-like Semiconductors Li(2)-CdGeS(4) and Li(2)CdSnS(4). *Inorg. Chem.* **2009**, *48*, 7516−7518.
(58) Zhang, J.-H.; Clark, D. J.; Weiland, A.; Stoyko, S. S.; Kim, Y. S.; Jang, J. I.; Aitken, J. A. Li2CdGeSe4and Li2CdSnSe4: Biaxial Nonlinear Optical Materials with Strong Infrared Second-Order Responses and Laser-Induced Damage Thresholds Influenced by Photoluminescence. *Inorg. Chem. Front.* **2017**, *4*, 1472−1484.
(59) Chen, M.-C.; Wu, L.-M.; Lin, H.; Zhou, L.-J.; Chen, L. Disconnection Enhances the Second Harmonic Generation Response: Synthesis and Characterization of Ba23Ga8Sb2S38. *J. Am. Chem. Soc.* **2012**, *134*, 6058−6060.
(60) Yin, W.; Zhou, M.; Iyer, A. K.; Yao, J.; Mar, A. Noncentrosymmetric Quaternary Selenide Ba23Ga8Sb2Se38: Synthesis, Structure, and Optical Properties. *J. Alloys Compd.* **2017**, *729*, 150−155.
(61) Zhang, Y.; Mei, D.; Yang, Y.; Cao, W.; Wu, Y.; Lu, J.; Lin, Z. Rational Design of a New Chalcogenide with Good Infrared Nonlinear Optical Performance: SrZnSnS4. *J. Mater. Chem. C* **2019**, *7*, 8556−8561.
(62) Pang, X.; Wang, R.; Che, X.; Huang, F. SrZnSnSe4: Synthesis, Crystal Structure and Nonlinear Optical Properties. *J. Solid State Chem.* **2021**, *297*, 122092.
(63) Guo, S.-P.; Cheng, X.; Sun, Z.-D.; Chi, Y.; Liu, B.-W.; Jiang, X.-M.; Li, S.-F.; Xue, H.-G.; Deng, S.; Duppel, V.; Köhler, J.; Guo, G.-C. Large Second Harmonic Generation (SHG) Effect and High Laser-induced Damage Threshold (LIDT) Observed Coexisting in Gallium Selenide. *Angew. Chem.* **2019**, *131*, 8171−8175.
(64) Li, S.-F.; Jiang, X.-M.; Liu, B.-W.; Yan, D.; Lin, C.-S.; Zeng, H.-Y.; Guo, G.-C. Superpolyhedron-Built Second Harmonic Generation Materials Exhibit Large Mid-Infrared Conversion Efficiencies and High Laser-Induced Damage Thresholds. *Chem. Mater.* **2017**, *29*, 1796−1804.
(65) Lin, H.; Zheng, Y.-J.; Hu, X.-N.; Chen, H.; Yu, J.-S.; Wu, L.-M. Non-Centrosymmetric Selenides $AZn_4in_5Se_{12}$(A=Rb, Cs): Synthesis, Characterization and Nonlinear Optical Properties. *Chem.—Asian J.* **2017**, *12*, 453−458.
(66) Lin, H.; Chen, L.; Zhou, L.-J.; Wu, L.-M. Functionalization Based on the Substitutional Flexibility: Strong Middle IR Nonlinear Optical Selenides AX(II)(4)X(III)(5)Se12. *J. Am. Chem. Soc.* **2013**, *135*, 12914−12921.
(67) Liu, B.-W.; Hu, C.-L.; Zeng, H.-Y.; Jiang, X.-M.; Guo, G.-C. Strong SHG Response via High Orientation of Tetrahedral Functional Motifs in Polyselenide $A_2Ge_4Se_{10}$(A = Rb, Cs). *Adv. Opt. Mater.* **2018**, *6*, 1800156.
(68) Li, X.-H.; Yao, W.-D.; Wei, Y.-L.; Guo, S.-P. Three-in-One Strategy Constructing a Series of Hybrid Tetrahedral Motif-Based Selenides with Balanced Second-Order Nonlinear Optical Performance. *Inorg. Chem.* **2021**, *60*, 6641−6648.
(69) Gao, L.; Xu, J.; Tian, X.; Zhang, B.; Wu, X.; Wu, K. $AgGaSe_2$-Inspired Nonlinear Optical Materials: Tetrel Selenides of Alkali Metals and Mercury. *Chem. Mater.* **2022**, *34*, 5991−5998.
(70) Zhang, J.-H.; Clark, D. J.; Weiland, A.; Stoyko, S. S.; Kim, Y. S.; Jang, J. I.; Aitken, J. A. Li2CdGeSe4and Li2CdSnSe4: Biaxial Nonlinear Optical Materials with Strong Infrared Second-Order Responses and Laser-Induced Damage Thresholds Influenced by Photoluminescence. *Inorg. Chem. Front.* **2017**, *4*, 1472−1484.
(71) Lin, H.; Chen, H.; Zheng, Y.-J.; Yu, J.-S.; Wu, X.-T.; Wu, L.-M. Two Excellent Phase-Matchable Infrared Nonlinear Optical Materials Based on 3D Diamond-like Frameworks: RbGaSn2Se6 and RbInSn2Se6. *Dalton Trans.* **2017**, *46*, 7714−7721.
(72) Dong, X.; Huang, L.; Zeng, H.; Lin, Z.; Ok, K. M.; Zou, G. High-Performance Sulfate Optical Materials Exhibiting Giant Second Harmonic Generation and Large Birefringence. *Angew. Chem., Int. Ed.* **2022**, *61*, No. e202116790.
(73) Abudurusuli, A.; Li, J.; Pan, S. A Review on the Recently Developed Promising Infrared Nonlinear Optical Materials. *Dalton Trans.* **2021**, *50*, 3155−3160.
(74) Ok, K. M.; Halasyamani, P. S.; Casanova, D.; Llunell, M.; Alemany, P.; Alvarez, S. Distortions in Octahedrally Coordinated d^0

https://doi.org/10.1021/acs.inorgchem.2c03852
Inorg. Chem. 2023, 62, 574−582

Transition Metal Oxides: A Continuous Symmetry Measures Approach. *Chem. Mater.* **2006**, *18*, 3176−3183.
(75) Ok, K. M. Toward the Rational Design of Novel Noncentrosymmetric Materials: Factors Influencing the Framework Structures. *Acc. Chem. Res.* **2016**, *49*, 2774−2785.
(76) Jiang, X.; Kang, L.; Luo, S.; Gong, P.; Lee, M.-H.; Lin, Z. Development of nonlinear optical materials promoted by density functional theory simulations. *Int. J. Mod. Phys. B* **2014**, *28*, 1430018.
(77) Tran, T. T.; Yu, H.; Rondinelli, J. M.; Poeppelmeier, K. R.; Halasyamani, P. S. Deep Ultraviolet Nonlinear Optical Materials. *Chem. Mater.* **2016**, *28*, 5238−5258.
(78) Li, Y. Y.; Wang, W.-J.; Wang, H.; Lin, H.; Wu, L.-M. Mixed-Anion Inorganic Compounds: A Favorable Candidate for Infrared Nonlinear Optical Materials. *Cryst. Growth Des.* **2019**, *19*, 4172−4192.
(79) Chen, H.; Wei, W.-B.; Lin, H.; Wu, X.-T. Transition-metal-based chalcogenides: A rich source of infrared nonlinear optical materials. *Coord. Chem. Rev.* **2021**, *448*, 214154.
(80) Chen, M.-M.; Zhou, S.-H.; Wei, W.-B.; Wu, X.-T.; Lin, H.; Zhu, Q.-L. Phase Matchability Transformation in the Infrared Nonlinear Optical Materials with Diamond-Like Frameworks. *Adv. Opt. Mater.* **2021**, *10*, 2102123.
(81) Yang, H.-D.; Ran, M.-Y.; Zhou, S.-H.; Wu, X.-T.; Lin, H.; Zhu, Q.-L. Rational design via dual-site aliovalent substitution leads to an outstanding IR nonlinear optical material with well-balanced comprehensive properties. *Chem. Sci.* **2022**, *13*, 10725−10733.

https://doi.org/10.1021/acs.inorgchem.2c03852
Inorg. Chem. 2023, 62, 574−582